Materials Science and Engineering C 75 (2017) 1366–1375

Contents lists available at ScienceDirect

Materials Science and Engineering C

journal homepage: www.elsevier.com/locate/msec

The effect of sliding onto the metal-electrolyte interface: Studying model parameter modifications by means of EIS

Josianne Cassar [a], Bertram Mallia [a], Andreas Karl [b], Joseph Buhagiar [a,*]

[a] Department of Metallurgy and Materials Engineering, University of Malta, Msida, MSD2080, Malta
[b] Bodycote Specialist Technologies GmbH, Landsberg, Germany

ARTICLE INFO

Article history:
Received 2 March 2017
Accepted 4 March 2017
Available online 6 March 2017

Keywords:
EIS
Tribocorrosion
CoCrMo alloy
S-phase
Carburizing
Expanded austenite
Cobalt-chromium alloy
ASTM F1537
Biomedical
Orthopaedic

ABSTRACT

Several problems are associated with corrosion-wear occurring on metal-on-metal hip implants made out of cobalt-chromium based alloys. Low temperature carburizing, a process that creates a hard and corrosion resistant diffused layer in Cobalt-Chromium-Molybdenum (CoCrMo) alloys, known as S-phase, may be a possible solution towards mitigating these problems. In this work, static- and tribo-corrosion testing involving an alumina versus CoCrMo (untreated and carburized) were conducted in Ringer's solution. Electrochemical impedance spectroscopy was used to compare impedance plots attained before and after sliding so as to understand how the metal-electrolyte interface is affected by rubbing. Both untreated and carburized CoCrMo experienced extensive reduction in corrosion resistance following sliding wear damage such that one should expect a considerably deteriorated performance of both surfaces in a tribocorrosion application. The structure of the interface was relatively unaffected after sliding at the equilibrium and passive potentials. This implies that the layers making up the interface before sliding were still present after sliding. However, their properties changed - the interface's real resistance dropped while its capacitance increased. The former was linked to a weaker, damaged passive film while the latter was linked to accumulation of wear debris and corrosion products.

1. Introduction

CoCrMo alloys are extensively utilised as biomaterials in hip replacements because of their good corrosion and wear resistance. However, several investigations report problems associated with the aforementioned alloys such as: high physiological level of the element cobalt, neurological impairment, inflammation, DNA damage and aseptic loosening [1–4]. These adverse effects associated with CoCrMo implants are consequences of corrosion and corrosion-wear. Both phenomena depend on the metal itself and the electrolyte with which it is in contact, in this case body fluids. Hence improving the tribocorrosion response of the surfaces in contact would be of great benefit. Such an improvement may be achieved by introducing carbon S-phase into the metal surface. The metastable, hard, supersaturated, precipitate-free S-phase, forms in low temperature surface treatments which introduce interstitial carbon, nitrogen or both, into octahedral locations in the substrate's lattice [5,6]. In this work a proprietary treatment owned by Bodycote Hardiff GmbH, Germany is used to introduce carbon S-phase. During this carburizing treatment, the metal is exposed to a temperature below 500 °C and very high carbon potential over several days; the resulting S-phase layer is very similar to that obtained through direct current and active screen low temperature carburizing [7]. The S-phase layer is also reported to have good cytocompatibility, as per Caligari Conti et al. [8]. In fact, the author states that S-phase on the CoCrMo alloy retains the untreated metal's excellent cytocompatibility.

Luo et al. [9] investigate the tribocorrosion behaviour of carbon S-phase on ASTM F1537 CoCrMo alloy when sliding against an 8 mm diameter alumina ball in Ringer's solution, with a normal force of 20 N and a frequency of 1 Hz. Lower total wear volumes were reported for the carburized specimens at cathodic and anodic potentials, while the opposite was true for OCP. The authors observe that degradation by mechanical wear dominates in both surface conditions at all potentials, even though the ratio of chemical to mechanical wear increases with increasing potentials. The authors state that the improvement in tribocorrosion behaviour resulted because of increased surface hardness after treatment. Moreover, the hard S-phase provides improved support to the passive film such that it can better withstand mechanical damage during tribocorrosion.

The effect of nitriding and carbonitriding on corrosion-wear of the same alloy was recently reported by Liu et al. [10]. The tests, conducted in Ringer's solution with a 30 N normal force at 1.12 Hz (WC/Co counter-body), indicate that corrosion-wear resistance improved with both surface treatments, with plasma nitriding producing a lower

* Corresponding author.
E-mail address: joseph.p.buhagiar@um.edu.mt (J. Buhagiar).

http://dx.doi.org/10.1016/j.msec.2017.03.048
0928-4931/

Table 1
Chemical composition of ASTM F1537 CoCrMo alloy.

Composition (wt%)												
C	Mn	Si	P	S	Cr	Ni	Mo	Cu	Co	N	W	Fe
0.05	0.80	0.62	0.003	0.0005	27.64	0.07	5.46	0.01	Bal.	0.169	0.02	0.2

wear loss compared to plasma carbonitriding. Lutz et al. [11] study tribocorrosion of nitrogen PIII CoCrMo sliding against a 4.8 mm diameter alumina ball in a simulated body fluid; a load of 1 N and sliding speed of 1.6 Hz were used. The investigation showed that reduction of the alloy's volumetric loss was associated with lower (<520 °C) treatment temperatures, as higher temperatures promote intense corrosion (because of nitride precipitation) resulting in high wear loss.

Corrosion and tribocorrosion are particularly linked to the point of contact between the metal and the solution. Hence, studying the metal-electrolyte interface through electrochemical impedance spectroscopy may indicate the structure, properties and reactions of the interface associated with corrosion-wear and consequently how to minimise the problems linked to it.

The research group of Universidad Politécnica de Valencia conducted comprehensive Electrochemical Impedance Spectroscopy (EIS) research on both low and high carbon CoCrMo alloys [12–17]. Equivalent Electrical Circuits (EEC) and their parameters have been modelled to accommodate the different metal-electrolyte interfaces that arise due to different test potentials, electrolytes and the presence of a wear scar. These conditions affect the structure and electrochemical properties of the metal-electrolyte interface [13].

The effect of sliding upon the resistance of the interface is also investigated by Mathew et al. [18] who depict Bode plots (A graph of the frequency response of a system) attained before and after rubbing wrought low carbon ASTM F1537 alloy against 10 mm and 28 mm diameters alumina balls with a 1 N force when submerged in Phosphate Buffered Solution (PBS). A considerable drop in resistance and impedance magnitude at low frequencies was attained; thus, sliding adversely affects the CoCrMo-PBS interface.

This work is novel in nature and is of scientific, medical and industrial importance. To date, all tribocorrosion studies coupled with EIS have been conducted on untreated CoCrMo alloys. This is because research on surface treated CoCrMo alloys only deal with volumetric losses. The aim of this work is to analyse the metal-electrolyte interface at three potentials (cathodic, equilibrium and passive potentials) and how it changes with a low temperature carburizing surface treatment. Furthermore, impedance spectra and model parameters attained before and after sliding are compared to better understand the effect of mechanical action on the alloy-electrolyte interface and relate to the tribocorrosion performance.

2. Materials and methods

2.1. Materials

A wrought ASTM F1537 CoCrMo (L. Klein, Switzerland) implant alloy whose chemical composition is given in Table 1 was used. Coupons 25.4 mm in diameter and 6.8 mm in thickness were cut from an annealed round bar by means of an electrical-discharge-wire cutting machine. In order to obtain flat and parallel surfaces the coupons were initially ground on a surface grinding machine. These coupons were metallographically prepared using silicon carbide paper of starting grit size of 120 up to 1200. The coupons were then polished to a surface finish of $R_a = 0.01$ μm using 6 μm and 3 μm diamond pastes and a suspension of 0.6 μm colloidal silica (MetPrep, UK).

2.2. Surface treatment

A low temperature carburizing surface treatment by Bodycote Hardiff GmbH (Landsberg, Germany) was applied to the polished coupons. This diffusion treatment creates a carbon S-phase layer [19] and results in a surface roughness of $R_a = 0.03$ μm.

2.3. Material characterisation

Prior to testing the surface treatment was characterised by Scanning Electron Microscopy, Glancing-Angle X-Ray Diffraction, Glow Discharge Optical Emission Spectroscopy and Micro hardness testing. Since this characterisation does not fall within the main scope of this work; more details can be found in the following reference: [19].

2.4. Electrochemical impedance spectroscopy

2.4.1. Cleaning procedure

Uniformity in the surface conditions of all coupons is essential in electrochemical impedance spectroscopy as this guarantees that every test starts off with the same surface conditions. In order to ensure this uniformity a 30-minute long cleaning procedure was adopted on each and every sample. This involved: cleaning with soap and water; a 15-minute ultrasonic cleaning in isopropyl alcohol; polishing with 3 μm diamond paste for 2 s enough to remove the passive film; and a 15-minute ultrasonic cleaning in isopropyl alcohol.

2.4.2. EIS equipment

EIS measurements involved the use of a three-electrode corrosion test cell, using a Gamry Instruments Reference 600™ (USA) potentiostat before sliding and a Gamry Interface 1000™ (USA) potentiostat after sliding. The three-electrode setup was made up of: a saturated calomel reference electrode housed in a Luggin probe, a platinum coated titanium counter electrode and the test coupon as the working electrode. 300 ml of Ringer's solution (Lab M, UK), whose chemical composition is given in Table 2 was used as an electrolyte. The solution had a pH of 7.4 and was kept at a temperature of 37 ± 1 °C.

For the impedance spectroscopy experiments an AC signal of 10 mV (rms) was used and the test frequency had a range of 10,000 Hz to 0.004 Hz with ten points per decade. The lower frequencies provide more information on the interface but also result in a longer measurement time which might compromise the stability of the system [19]. Every test condition was repeated for at least four times and equivalent electrical circuits (EECs) were modelled by means of the Simplex mathematical algorithm.

Table 2
Composition of Ringer's solution.

	NaCl	KCl	$CaCl_2$	$NaHCO_3$
g l^{-1}	9.00	0.42	0.48	0.20
Molarity	0.1540	0.0560	0.0043	0.0024

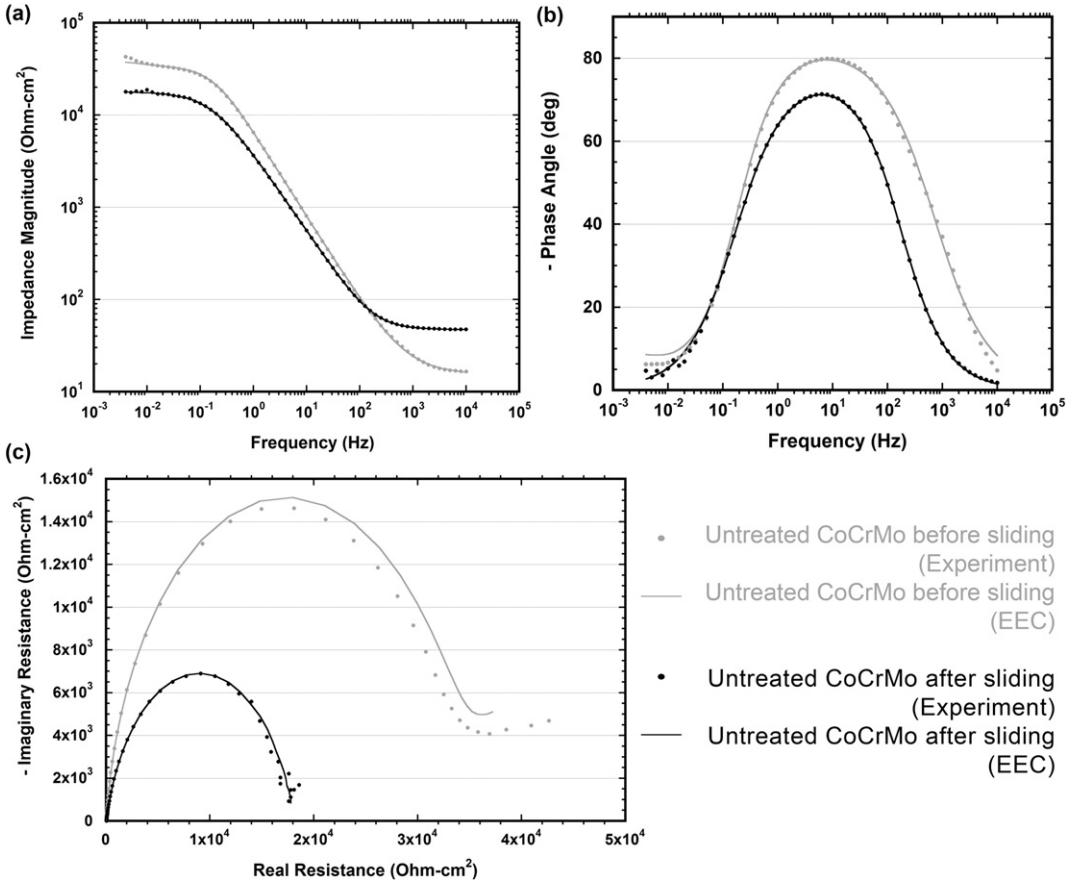

Fig. 1. EIS (a) Bode-magnitude, (b) Bode-phase and (c) Nyquist plots comparing the response of untreated CoCrMo before and after sliding when the cell was polarised at a cathodic potential of −0.7 V_{SCE}.

2.4.3. Potentials

EIS tests were conducted at various potentials which were selected according to Open Circuit Potential (OCP) trends recorded for both untreated and carburized alloys. The chosen potentials correspond to different chemical conditions at the interface:

- Cathodic (−0.7 V vs. SCE reference): At this potential, the passive film on the metal is not growing, such that the passive film present on the surface is that generated before the sample is inserted into the electrochemical cell. Consequently, the resulting resistance is expected to be quite low. Since this voltage deviates from the equilibrium potential, one expects cathodic reactions to dominate at the metal-electrolyte interface and possibly, mass transport or diffusion;
- OCP (0 V vs. OCP): the equilibrium potential is associated with a balance of anodic and cathodic reactions and therefore, the reactions taking place at the interface balance each other. One expects that the passive film and the electrical double layer (EDL) are present at this potential, and hence the resistance is expected to be significantly higher than that at the cathodic potential;
- Passive (0.1 V vs. SCE reference): This potential is associated with the presence of a protective passive film. Therefore, at this voltage one expects that the interface is composed of a stable and established passive film (with a corresponding high resistance) together with the Electrical Double Layer (EDL).

2.4.4. EIS procedure before sliding

The tests at cathodic potential were carried out by first monitoring the OCP of the electrochemical cell for 10 min, followed by polarisation at a cathodic potential of −0.7 V vs. SCE reference for 50 min, after which EIS testing was carried out at −0.7 V vs. SCE reference. The same procedure was used for the passive potential tests, but the cell was polarised to 0.1 V vs. SCE reference. The EIS tests at OCP involved one-hour monitoring of the OCP before the impedance was measured at this potential. The voltage of the EIS test was the last measured value established during the preceding hour of OCP monitoring.

2.4.5. EIS procedure after sliding

The tribocorrosion equipment used involved ball-on-disc reciprocating sliding motion at a frequency of 2 Hz and a stroke length of 6.5 mm. The bidirectional movement was achieved by a stationary polycrystalline alumina ball with a diameter of 12.7 mm. The material's hardness is very high namely 1700 HV and this is reflected in its high wear resistance, which implies that the ball's material loss is expected to be minimal. Furthermore, since alumina is a ceramic material, any galvanic coupling with the sample is avoided so that the current output from the test reflects solely the reactions taking place at the sample's surface and not at the ball. A three-electrode setup consisting of the tested sample as the working electrode, a saturated calomel reference electrode and a platinum coated titanium counter electrode was used. The exposed surface area in the tribo cell was 3.464 cm^2 and the electrodes were connected to Gamry's Interface 1000™ (USA) potentiostat. All parts in contact with the fluid including the ball holder and rod, were made of insulating materials (PTFE and Glass) to avoid any electrochemical corrosion which interferes with the experiments. The load utilised during these tests was set to 8 N. This load does not result in gross yielding of the test material at the contact. The container housing the electrodes was water-jacketed so that the 300 ml of Ringer's solution within was maintained at 37 °C (±1 °C).

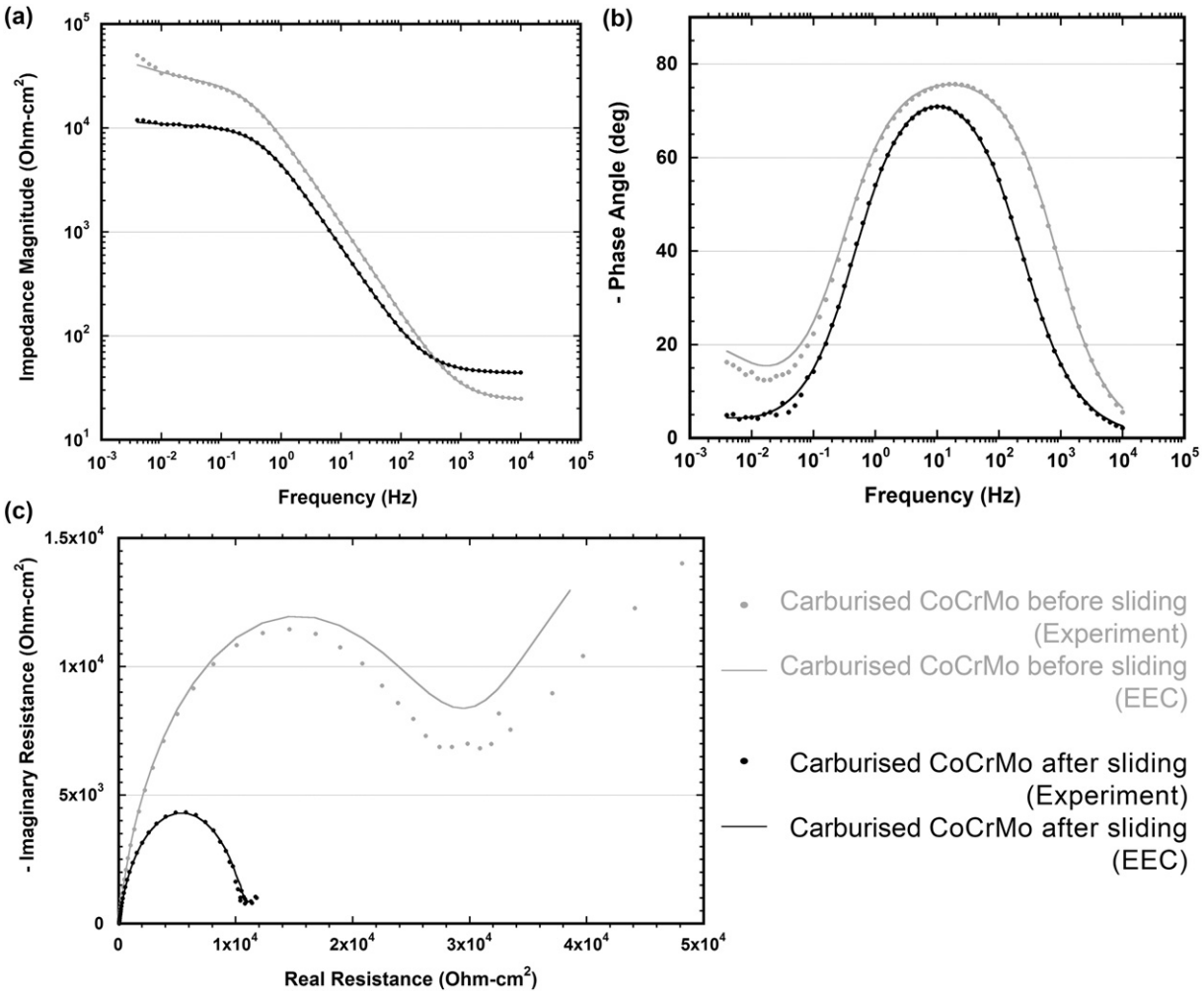

Fig. 2. EIS (a) Bode-magnitude, (b) Bode-phase and (c) Nyquist plots comparing the response of carburized CoCrMo before and after sliding when the cell was polarised at a cathodic potential of −0.7 V_{SCE}.

Initially, the electrochemical cell was exposed to the potential of the test (−0.7 V_{SCE}, OCP or 0.1 V_{SCE}) for 20 min and this was followed by 2 h of sliding where the same potential was maintained (floating potential in case of OCP) and during which the frictional force is measured. Afterwards, the rubbing was stopped and the test sample in contact with the Ringer's solution was left exposed to the test potential of the test for another 20 min. This was followed by an EIS procedure with parameters identical to those used before sliding. The EIS measurements were made using the potential that was utilisied throughout the tribocorrosion test. In the case of OCP, the potential utilised was the last one established before commencement of the EIS measurements.

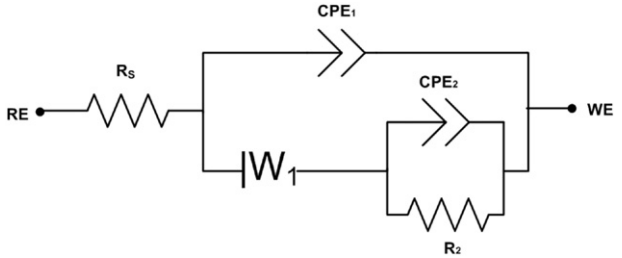

Fig. 3. Circuit including Warburg impedance, fitted to cathodic potential plots (EEC1).

Note that the tests were repeated at least four times for every potential and surface condition.

3. Results and discussion

3.1. Characterisation

The carburizing treatment resulted in a diffusion layer with a carbon interstitial content decreasing gradually from 8 wt% (and a hardness of 962 ± 5 $HV_{0.2}$) at the surface to 0.05 wt% (and a hardness of 473 ± 3 $HV_{0.2}$) at 10.5 μm below the surface. The hardness and chemical depth profiles together with phase analysis showed that a precipitate-free metastable supersaturated solid solution layer of carbon (S-phase or Expanded Austenite) was formed in the CoCrMo alloy. Detailed information of this layer can be obtained from reference: [19].

3.2. Cathodic potential

Figs. 1 and 2 compare the plots obtained before and after sliding for both untreated and carburized CoCrMo respectively at the cathodic potential of −0.7 V_{SCE}. At the cathodic potential one expects cathodic reactions to prevail and thus, an associated diffusion of oxygen from the solution to the interface could be present. Furthermore, one expects the presence of an Electrical Double Layer (EDL)

Table 3
Parameters obtained when modelling the untreated metal interface with EEC1, when polarised at a cathodic potential of −0.7 V_{SCE}.

	Before sliding	After sliding
R_s (Ω-cm^2)	18.24 ± 0.75	47.20 ± 0.45
Q_1 (μS-s$^\alpha$/cm^2)	13.36 ± 2.12	35.94 ± 0.70
α_1	0.88 ± 0.03	0.78 ± 0.005
Y_{O1} (μS√s/cm^2)	933.90 ± 134.60	92.29 ± 120.00
B_1 (√s)	18.45 ± 0.0006	21.64 ± 0.05
R_2 (kΩ-cm^2)	32.79 ± 0.63	18.00 ± 0.17
Q_2 (μS-s$^\alpha$/cm^2)	14.25 ± 1.98	19.52 ± 0.55
α_2	0.97 ± 0.02	0.93 ± 0.006
GoF	1.18×10^{-3}	213.80×10^{-6}

Table 4
Parameters obtained when modelling the carburized metal interface with EEC1, when polarised at a cathodic potential of −0.7 V_{SCE}.

	Before sliding	After sliding
R_s (Ω-cm^2)	24.19 ± 1.41	43.38 ± 0.50
Q_1 (μS-s$^\alpha$/cm^2)	20.83 ± 2.64	5.33 ± 0.92
α_1	0.87 ± 0.03	0.36 ± 0.07
Y_{O1} (μS√s/cm^2)	361.60 ± 20.70	38.23 ± 10.19
B_1 (√s)	19.78 ± 0.01	1.32 ± 0.006
R_2 (kΩ-cm^2)	27.03 ± 0.60	10.70 ± 0.73
Q_2 (μS-s$^\alpha$/cm^2)	2.13 ± 1.16	38.60 ± 0.55
α_2	0.97 ± 0.19	0.87 ± 0.003
GoF	1.85×10^{-3}	199.50×10^{-6}

Table 5
Parameters obtained when modelling the untreated metal interface with EEC2, obtained at OCP.

	Before sliding	After sliding
R_s (Ω-cm^2)	24.50 ± 0.28	45.18 ± 0.49
R_1 (kΩ-cm^2)	257.30 ± 9.37	17.56 ± 5.08
Q_1 (μS-s$^\alpha$/cm^2)	31.75 ± 1.17	85.80 ± 42.25
α_1	0.95 ± 0.01	0.94 ± 0.06
C_1(μF/cm^2)	21.78	60.18
R_2 (kΩ-cm^2)	609.80 ± 32.95	104.30 ± 14.90
Q_2 (μS-s$^\alpha$/cm^2)	38.68 ± 1.42	42.61 ± 10.88
α_2	0.91 ± 0.01	0.84 ± 0.01
C_2(μF/cm^2)	52.87	56.61
GoF	1.61×10^{-3}	649.20×10^{-6}

Table 6
Parameters obtained when modelling the carburized metal interface with EEC2, obtained at OCP.

	Before sliding	After sliding
R_s (Ω-cm^2)	24.07 ± 0.25	44.13 ± 0.44
R_1 (kΩ-cm^2)	330.7 ± 77.80	18.15 ± 5.99
Q_1 (μS-s$^\alpha$/cm^2)	25.57 ± 3.93	133.10 ± 66.11
α_1	0.90 ± 0.004	0.93 ± 0.01
C_1(μF/cm^2)	11.25	90.40
R_2 (kΩ-cm^2)	1071.00 ± 111.9	218.10 ± 11.14
Q_2 (μS-s$^\alpha$/cm^2)	47.66 ± 12.87	37.06 ± 4.32
α_2	1.00 ± 0.04	0.95 ± 0.03
C_2(μF/cm^2)	47.66	41.37
GoF	2.23×10^{-3}	92.55×10^{-6}

but not that of the passive film, even though traces of this latter film could still be present at the interface since this film grows between polishing and commencement of EIS. The Bode-magnitude plots shown in Figs. 1(a) and 2(a) point towards the presence of a capacitor (negative slope curve in the middle frequencies) and resistors (curve becomes horizontal at middle and high frequencies, such that a constant impedance magnitude is associated with this range of frequencies). This is confirmed through the Nyquist (a parametric plot of a frequency response where the real part of the transfer function is plotted on the x-axis and the imaginary part is plotted on the y-axis) and Bode-phase plots as the former contain a semi-circle while the latter contain a maximum close to 90°. Therefore, these observations confirm the presence of a time constant. The Nyquist plots contain a straight diagonal line at low frequencies representing diffusion; thus, it appears that the phenomenon is present at the interface and it constitutes another time constant [20].

Table 7
Parameters obtained when modelling the untreated metal interface with EEC2, when polarised at a passive potential of 0.1 V_{SCE}.

	Before sliding	After sliding
R_s (Ω-cm^2)	18.14 ± 0.30	47.76 ± 0.44
R_1 (kΩ-cm^2)	85.39 ± 16.00	86.77 ± 4.46
Q_1 (μS-s$^\alpha$/cm^2)	44.23 ± 5.70	48.94 ± 2.82
α_1	0.89 ± 0.17	0.85 ± 0.004
C_1(μF/cm^2)	18.33	16.80
R_2 (kΩ-cm^2)	2774.00 ± 454.40	2060.00 ± 115.4
Q_2 (μS-s$^\alpha$/cm^2)	13.87 ± 5.09	37.68 ± 1.09
α_2	0.90 ± 0.08	0.96 ± 0.01
C_2(μF/cm^2)	20.81	45.17
GoF	1.40×10^{-3}	274.00×10^{-6}

Table 8
Parameters obtained when modelling the carburized metal interface with EEC2, when polarised at a passive potential of 0.1 V_{SCE}.

	Before sliding	After sliding
R_s (Ω-cm^2)	18.97 ± 0.29	41.18 ± 0.41
R_1 (kΩ-cm^2)	169.2 ± 38.99	145.90 ± 47.79
Q_1 (μS-s$^\alpha$/cm^2)	32.45 ± 7.47	61.83 ± 13.05
α_1	0.83 ± 0.007	0.86 ± 0.007
C_1(μF/cm^2)	7.14	23.38
R_2 (kΩ-cm^2)	3419.00 ± 247.10	2211.00 ± 261.60
Q_2 (μS-s$^\alpha$/cm^2)	17.73 ± 1.94	47.16 ± 6.96
α_2	0.97 ± 0.02	0.99 ± 0.03
C_2(μF/cm^2)	20.13	49.43
GoF	370.60×10^{-6}	75.07×10^{-6}

The experimental plots were modelled with the Equivalent Electrical Circuit termed EEC1 (Fig. 3), which was used by Fonseca et al. [21] to study the metal-electrolyte interface of titanium in PBS solution. The untreated and carburized surfaces were modelled by the same Equivalent Electrical Circuit (EEC) for a particular condition since it was assumed that the components of the interface of both surfaces would be the same. The discrepancy between the two surfaces would hence be in the circuit parameter values rather than the model itself. Using the same EEC is also required for comparison purposes.

The EEC model contains a constant phase element (CPE) instead of perfect capacitance, since the phenomenon of time constant dispersion is highly probable. Variation in current, potential and reactivity occurring along the electrode surface leads to time constant dispersion, as well as distributed properties of oxide layers [19,22].

Note that the EIS plots depicted in this section correspond to one test which is the best representative of all tests carried out at that particular condition. Furthermore, EEC parameter errors correspond to the chosen (best representative) plot only, and relate the discrepancy between the actual EIS plot (result) and the EEC fit (model).

The Warburg impedance element represents diffusion of oxygen from the electrolyte to the interface resulting in the following possible reaction [12,23]:

$$O_2 + 2H_2O + 4e^- \rightarrow 4OH^-$$

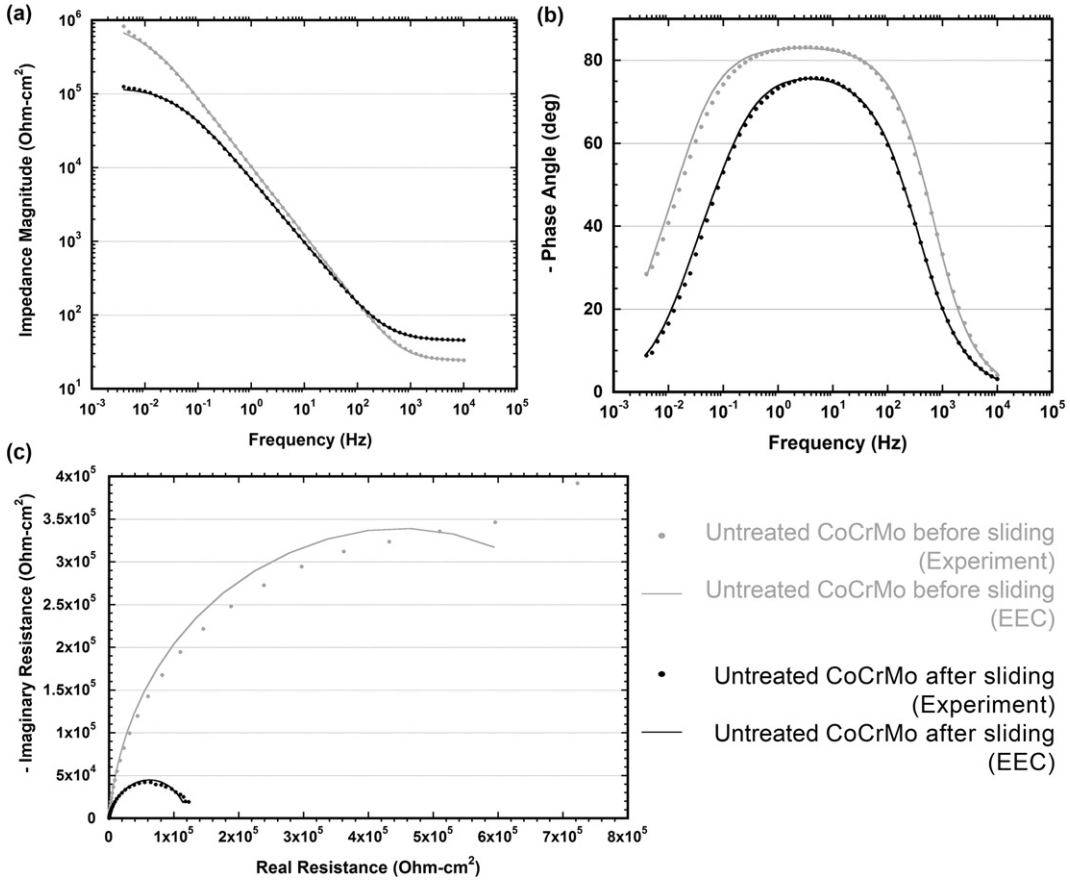

Fig. 4. EIS (a) Bode-magnitude, (b) Bode-phase and (c) Nyquist plots comparing the response of untreated CoCrMo at OCP; before (OCP = −0.335 V_{SCE}) and after (OCP = −0.360 V_{SCE}) sliding.

CPE_1 is associated with the diffusion layer and is hence representative of capacitance dispersion occurring across this layer. Note that the Warburg impedance and CPE_1, both associated with diffusion, are next to the reference electrode, thus on the outer side of the interface. The RC combination of R_2 and CPE_2 is associated with the EDL and possible traces of the passive film; R_2 represents the charge transfer resistance across this layer while CPE_2 is the capacitance of the double layer.

The shape of all plots in Figs. 1 and 2 is reasonably similar, with diffusion being much more pronounced in the plots obtained before sliding. The overall impedance of the interfaces after sliding is lower than that obtained before sliding, as evidenced in the Nyquist plots and Bode-magnitude plots. The maxima of the Bode-phase plots obtained before sliding are higher than those obtained after sliding, which implies that time constant dispersion in the former cases is lower than that in the latter cases. The parameters attained after modelling the untreated and carburized samples' impedance response with the Equivalent Electrical Circuit termed EEC2 are listed in Tables 3 and 4, respectively. Note that the goodness of fit represents the Chi-squared value divided by the total number of points in the spectra [24].

The real resistance after sliding is lower compared to that obtained before sliding. The CPE linked to real resistance, CPE_2, experiences a slight increase in CPE constant after sliding, and an associated decrease in CPE exponent, which implies that time constant dispersion increased after sliding. The CPE_1 constant and exponent differ considerably as well, and this may be linked to variation in diffusion between the two interfaces. In fact, the discrepancy is also shown through the Warburg coefficient σ as that before sliding was calculated to be 757.15 Ω-$cm^2/s^{1/2}$ while that after sliding was found to be 7.66 Ω-$cm^2/s^{1/2}$, and this is evidenced by the diffusion part of the Nyquist plot.

Similarly to the previous case, the real resistance is lower after sliding. In addition, the CPE_2 constant increased after sliding, while the CPE_2 exponent decreased, with the latter modification indicating an increase of time constant dispersion on the worn surface. The CPE_1 constant and exponent differ considerably as these are related to discrepancy in diffusion between the two interfaces, reflected also in Y_{O1} and B_1 parameters. The values of the Warburg coefficient σ, confirm these observations, as that calculated before sliding was 1955.49 Ω-$cm^2/s^{1/2}$ while that obtained after sliding was 18.50 Ω-$cm^2/s^{1/2}$.

3.3. Open circuit potential

Impedance spectra obtained before and after sliding at OCP for untreated and carburized CoCrMo are shown in Figs. 4 and 5. At OCP, the metal is in equilibrium which implies that the cathodic and anodic reactions are balanced. The lack of prevalence of any of the two types of reactions suggests that diffusion will not be shown in the spectra. The presence of the EDL and the passive film is expected at this potential, with the latter being particularly pronounced since it is free to grow at the interface. As a consequence, two RC time constants are expected in the spectra since these two layers have resistive and capacitive characteristics.

The Bode and Nyquist plots shown in Figs. 4 and 5 indicate the presence of capacitive behaviour in the middle and lower frequencies, as well as resistance, particularly at the lower frequencies of the untreated plots. The three plots seem to indicate the presence of one time constant only which suggests that superposition of time constants occurred.

The confirmation that two time constants are superimposed comes from the plots in Fig. 6, which represents the interface of an unpolished surface having a stable passive film formed in air. The

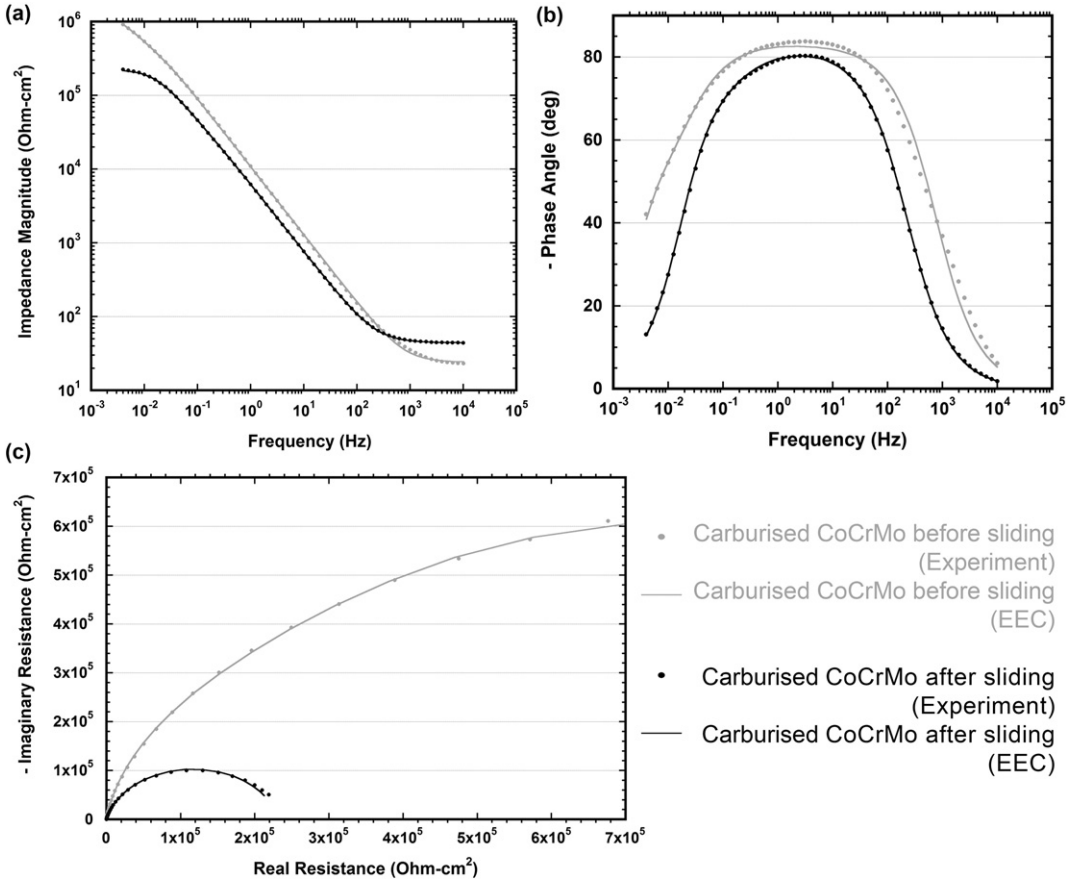

Fig. 5. EIS (a) Bode-magnitude, (b) Bode-phase and (c) Nyquist plots comparing the response of carburized CoCrMo at OCP; before (OCP = −0.111 V_{SCE}) and after (OCP = −0.220 V_{SCE}) sliding.

plots in Figs. 4 and 5 represent a sample which is freshly polished before immersion, and thus the passive film is still growing during EIS, which implies that its resistance and capacitance are still (relatively) low. Consequently, its time constant is similar to that of the EDL which established itself upon contact between the metal and solution, hence, superposition of time constants occurred.

When a sample which was not polished for a long time is inserted into the cell (Fig. 6), its passive film, which formed in air, is stable and highly resistive and this is reflected upon its RC time constant value, which differs from that of the former situation. In this case, the time constant of the passive film and EDL are not similar and so, two separate maxima in the Bode-phase angle plot appear, hence the presence of two time constants. Note that this is evidenced only in the Bode-phase angle, thus highlighting the importance of analysing all three plots during EIS.

All plots were modelled using the Equivalent Electrical Circuit termed EEC2 shown in Fig. 7, which contains two RC time constants in series. The outer combination R_1 and CPE_1 is associated with the charge transfer resistance and capacitance of the EDL (outer layer), while R_2 and CPE_2 represent the resistance and capacitance of the passive film (a consequence of movement of charged species and vacancies within the film), and are thus closer to the Working Electrode (WE). The polarisation resistance of the interface is the summation of R_1 and R_2, which corresponds to the point at which the semi-circle in Nyquist plots crosses the x-axis [12]. The resistance of the solution between the Working Electrode (WE) and the Reference Electrode (RE) is represented by the resistive element, R_S. The CPE parameter is converted into capacitance to associate changes in this parameter with possible modifications of the layers' dielectric constant and thickness [19].

In general, the shapes of all plots (Figs. 4 and 5) are similar. The Nyquist plots clearly show that the impedance of the interfaces before sliding is higher than that after sliding, with this being particularly evident in the untreated CoCrMo plots. The Bode-phase angle plots of the interfaces before sliding are wider (less superposition of time constants) and higher (lower time constant dispersion) than the plots obtained after sliding. Tables 5 and 6 list the parameters values attained during EEC2 modelling of the untreated and carburized impedance spectra, respectively.

The parameter values confirm that the interface's real resistance before sliding is higher than that after sliding, for both the EDL and the passive film. Capacitance of the passive film before and after sliding shows that the latter film has a slightly higher value which implies that either the film after sliding is thinner, or else, that it has a higher dielectric constant. The EDL capacitance is lower before sliding compared to that obtained after sliding. Hence, the EDL established after sliding may be thinner than that established before sliding or else, the former has a higher dielectric constant. The CPE_1 exponent is similar in both cases; however, CPE_2 exponent indicates that the passive film on the worn surface has a higher time constant dispersion compared to the unworn surface.

As the Nyquist plots indicate, the real resistance of both layers in the carburized metal-electrolyte interface is lower after sliding compared to that attained before sliding. Another major discrepancy between the two is evidenced in the capacitance of the EDL, which is higher after sliding. This may imply that the EDL thickness after sliding is smaller than that before sliding, or else, that the EDL dielectric constant after sliding is higher than that before sliding. Time constant dispersion of

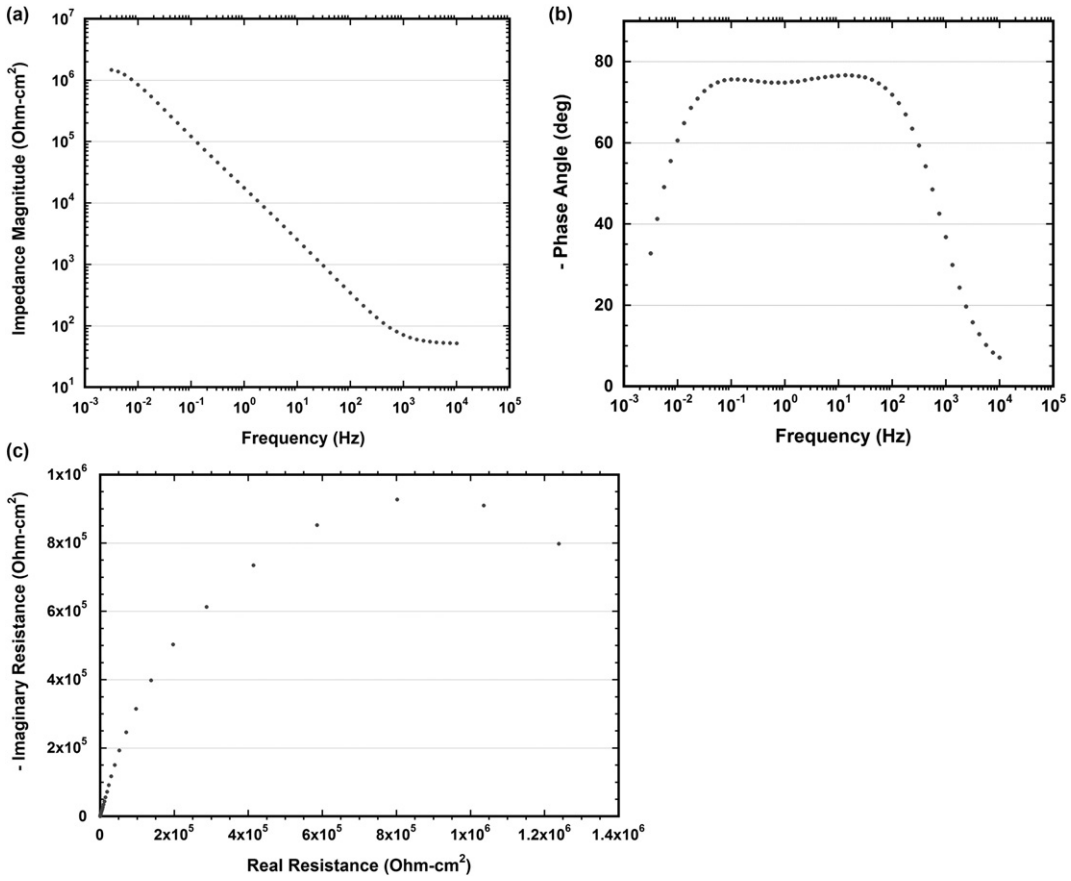

Fig. 6. EIS (a) Bode-magnitude, (b) Bode-phase and (c) Nyquist plots representing the interface of unpolished untreated CoCrMo at OCP (OCP = −0.446 V_{SCE}).

this layer is relatively similar in both situations. But when it comes to α_2, it is evident that the passive film loses its ideal capacitor behaviour after sliding since the exponent deviates from unity to 0.95. Hence, the wear scar on the carburized sample's surface was a major contributor in increasing the time constant dispersion in the metal's passive film, which could have caused a reduction in interface impedance. The passive film capacitance decreases after sliding, which may imply that the layer thickness increased, or else, that the layer has a lower dielectric constant.

3.4. Passive potential

Figs. 8 and 9 compare the impedance response obtained before and after sliding at 0.1 V_{SCE} for untreated and carburized CoCrMo respectively. At this potential, both samples are into the passive region and so, the passive film forms an integral part of the metal-electrolyte interface. One expects that this layer is more stable compared to OCP and also, that it has the highest resistance out of the three potentials. Similarly

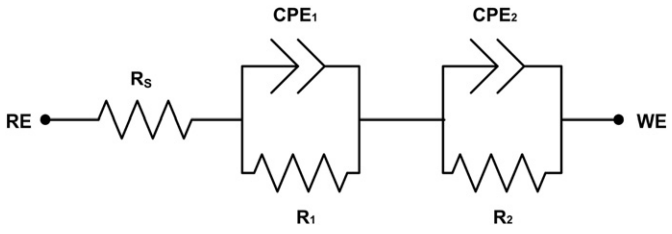

Fig. 7. Two RC combinations in series (EEC2).

to OCP, the interface consists of the passive film and the EDL, therefore two RC time constants. In addition, since this potential deviates from OCP, the anodic reactions prevailed over the cathodic reactions which could possibly introduce diffusion of metal ions out of the interface (to the solution). However, diffusion is minimal because the chosen potential is relatively close to the equilibrium potential. Therefore, the Equivalent Electrical Circuit termed EEC2 was used to model the interface; R_1 and CPE_1 are associated with the charge transfer resistance and capacitance of the double layer while R_2 and CPE_2 are associated with the resistance and capacitance of the passive film.

The shapes of the Bode-magnitude and Nyquist plots attained before and after sliding are almost the same for both surface conditions. The magnitude of the impedance before sliding is slightly higher than that after sliding, as shown in the Bode-magnitude curves. The length of the semi-circle curve in Nyquist plots, hence the impedance, is higher before sliding compared to after sliding for both untreated and carburized CoCrMo metals. The Bode-phase plots of the carburized samples are similar, with that obtained before sliding having a wider maximum than that obtained after sliding. This is also evident in the Bode-phase plots of the untreated samples; in addition, these plots differ in the lowest frequencies, with the plots obtained before sliding yielding lower phase angle values at these frequencies. Tables 7 and 8 compare the interface parameters attained before and after sliding.

The EDL real resistance is negligibly higher after sliding compared to that attained before sliding. The calculated capacitance of the EDL before and after sliding is similar, but α_1 differs slightly, as the EDL established before sliding has less time constant dispersion than that established after sliding.

Passive film resistance before sliding is higher than that obtained after sliding. The layer's capacitance associated with the worn CoCrMo

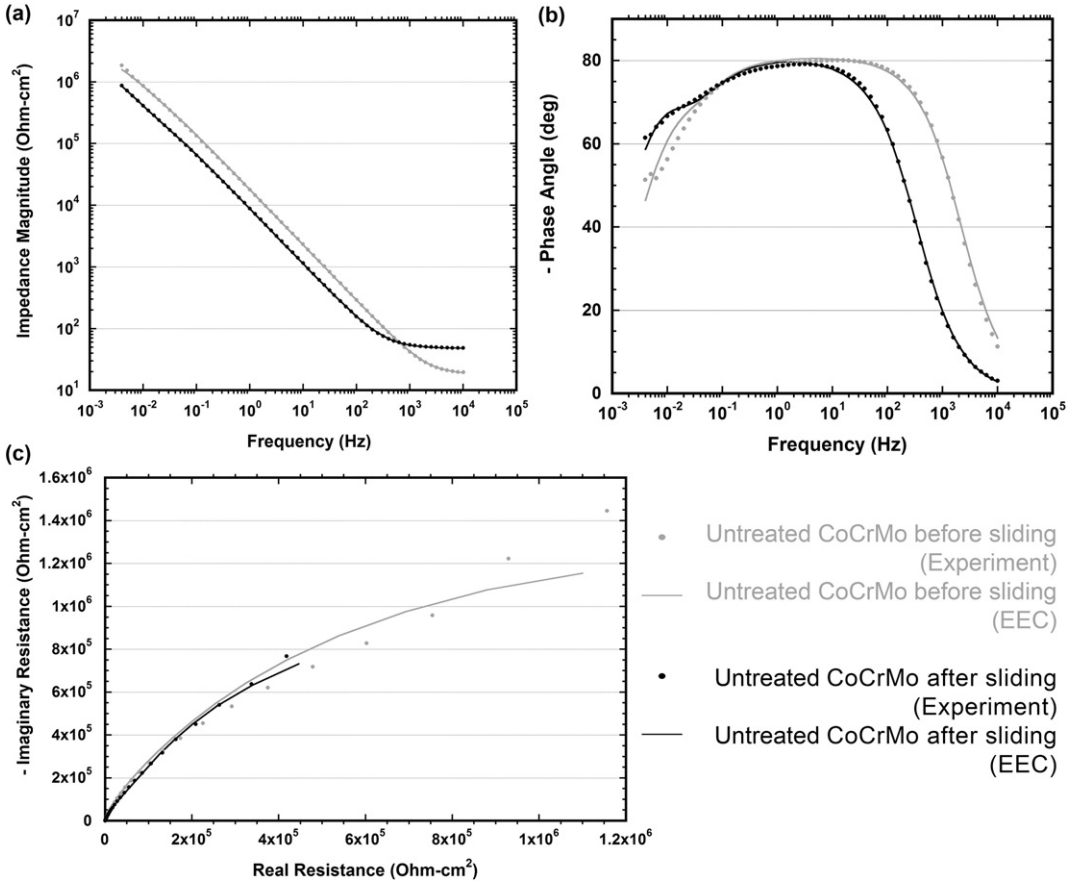

Fig. 8. EIS (a) Bode-magnitude, (b) Bode-phase and (c) Nyquist plots comparing the response of untreated CoCrMo before and after sliding when the cell was polarised at a passive potential of 0.1 V_{SCE}.

alloy is double that of the unworn CoCrMo alloy; therefore, the former may be thinner than the latter, or else, it has a higher dielectric constant. Capacitance increase after sliding was also noticed by other authors, who used EIS to investigate the interface of a scarred metal [25–27]. The authors tend to agree that this modification is a consequence of a change in the structure and dielectric constant of the layers within the interface due to an accumulation of wear debris and corrosion products. This also applies to the increase in capacitance after sliding of the EDL when the interface was not polarised (Tables 5 and 6). Interestingly, CPE_2 exponent of the passive film after sliding is higher than that obtained before sliding.

In this situation, one is comparing a complete S-phase surface before sliding, with an interrupted carburized layer (with some untreated CoCrMo alloy exposed) after sliding, as rubbing caused considerable damage to the S-phase. The real resistance associated with the passive film decreased considerably after sliding; however, the reduction was much less pronounced in the case of the EDL. The calculated capacitances of both the EDL and passive film increase after sliding; in fact, the layers' capacitances before sliding are less than half those obtained after sliding. Hence, the layers may be thicker before sliding, or else, they may have a higher dielectric constant after sliding. The pronounced increase in capacitance after sliding was also noticed by other authors, who claim that the increase is a consequence of the accumulation of wear debris and corrosion products [25–27]. Both CPE exponents are slightly higher after sliding, which implies a slightly lower time constant dispersion in the EDL and passive films on the treated, worn surface.

When one compares the drop in real resistance of the passive film, it is noticeable that this is higher for the carburized interface (1208 kΩ-cm^2) than for the untreated interface (714 kΩ-cm^2), even though the final resistance is slightly higher for the carburized CoCrMo alloy. Therefore, the deterioration in corrosion resistance after tribocorrosion is more evident in the carburized sample. The fact that a good part of the carburized metal's wear scar was made of untreated CoCrMo and not S-phase may have enhanced further the drop in resistance.

4. Conclusion

- Sliding was detrimental to the overall impedance of the metal-electrolyte interface in both surface conditions at all potentials. This implies that rubbing is expected to reduce the corrosion resistance of untreated and carburized CoCrMo alloy considerably, thus leading to a deteriorated performance of both surface conditions;
- When the electrochemical cell was polarised at the cathodic potential, the diffusion layer was significantly reduced after sliding, as the diagonal line in Nyquist plots associated with diffusion was almost eliminated. The overall interface impedance was also greatly reduced;
- Sliding did not change the structure of the metal-electrolyte interface at the equilibrium and passive potentials, but it affected the model parameter values. The interfaces' real resistance was significantly reduced while capacitance increased; the former was linked to a weaker, damaged passive film while the latter was linked to accumulation of wear debris and corrosion products.

Acknowledgments

This research was funded by the scholarship scheme “Strategic Educational Pathways Scholarship” (STEPS). The authors would like to thank ERDF (Malta) for financing the testing equipment through the project: “Developing an Interdisciplinary Material Testing and Rapid

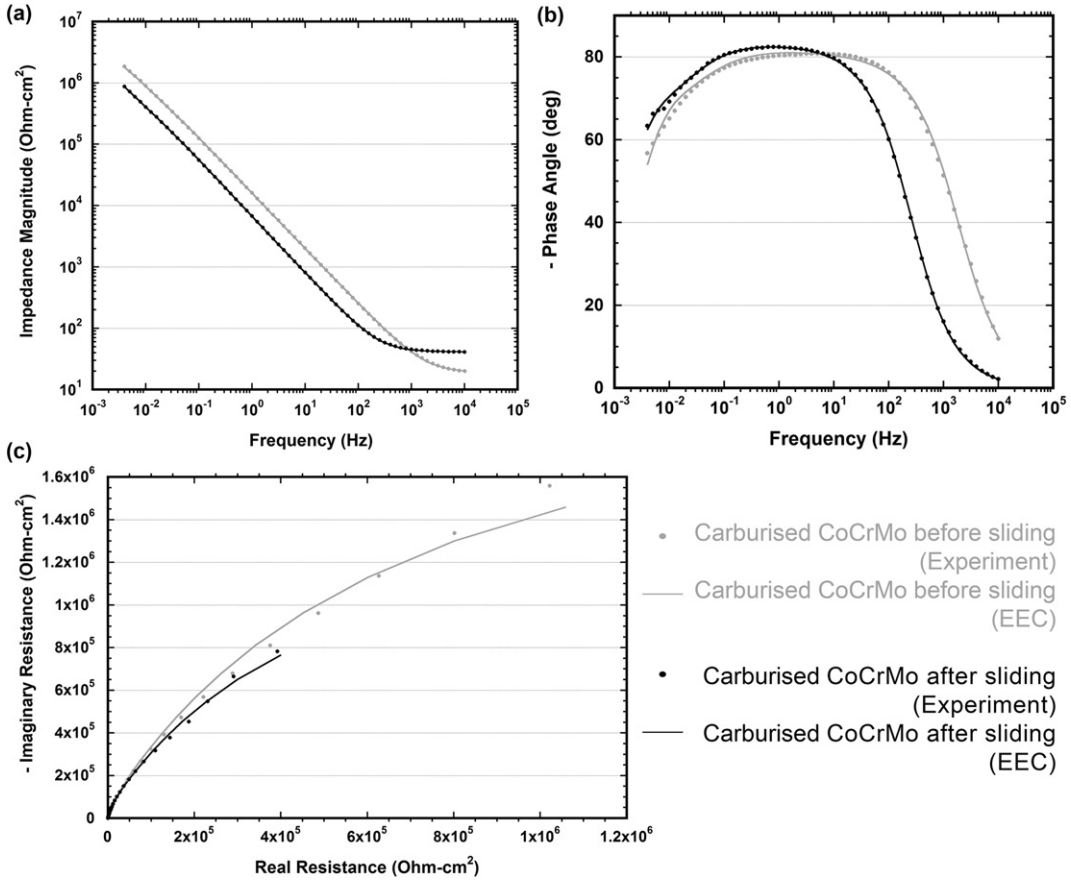

Fig. 9. EIS (a) Bode-magnitude, (b) Bode-phase and (c) Nyquist plots comparing the response of carburized CoCrMo before and after sliding when the cell was polarised at a passive potential of 0.1 V_{SCE}.

Prototyping R&D Facility (Ref. no. 012)". The authors are grateful for financial support received from Bodycote Hardiff GmbH, the Faculty of Engineering THINK10K grant and the University of Malta Research Fund.

References

[1] A.J. Smith, P. Dieppe, K. Vernon, M. Porter, A.W. Blom, Failure rates of stemmed metal-on-metal hip replacements: analysis of data from the National Joint Registry of England and Wales, Lancet 379 (2012) 1199–1204.
[2] J.R. Campbell, M.P. Estey, Metal release from hip prostheses: cobalt and chromium toxicity and the role of the clinical laboratory, Clin. Chem. Lab. Med. 51 (2012) 213–220.
[3] H.S. Gill, G. Grammatopoulos, S. Adshead, E. Tsialogiannis, E. Tsiridis, Molecular and immune toxicity of CoCr nanoparticles in MoM hip arthroplasty, Trends Mol. Med. 18 (2012) 145–155.
[4] A.P. Davies, A. Sood, A.C. Lewis, R. Newson, I.D. Learnmonth, C.P. Case, Metal-specific differences in levels of DNA damage caused by synovial fluid recovered at revision arthroplasty, J. Bone Joint Surg. (Br.) 87B (2005) 1439–1444.
[5] H. Dong, S-phase surface engineering of Fe-Cr, Co-Cr and Ni-Cr alloys, Int. Mater. Rev. 55 (2010) 65–98.
[6] X.Y. Li, S. Thaiwatthana, H. Dong, T. Bell, Thermal stability of carbon S phase in 316 stainless steel, Surf. Eng. 18 (2002) 448–452.
[7] J. Buhagiar, A. Spiteri, M. Sacco, E. Sinagra, H. Dong, Augmentation of crevice corrosion resistance of medical grade 316LVM stainless steel by plasma carburising, Corros. Sci. 59 (2012) 169–178.
[8] M. Caligari Conti, A. Karl, P. Schembri Wismayer, J. Buhagiar, Biocompatibility and characterization of a Kolsterised® medical grade cobalt-chromium-molybdenum alloy, Biomatter 4 (2014), e27713.
[9] X. Luo, X. Li, Y. Sun, H. Dong, Tribocorrosion behavior of S-phase surface engineered medical grade Co–Cr alloy, Wear 302 (2013) 1615–1623.
[10] R. Liu, X. Li, X. Hu, H. Dong, Surface modification of a medical grade Co-Cr-Mo alloy by low-temperature plasma surface alloying with nitrogen and carbon, Surf. Coat. Technol. 232 (2013) 906–911.
[11] J. Lutz, S. Mändl, Reduced tribocorrosion of CoCr alloys in simulated body fluid after nitrogen insertion, Surf. Coat. Technol. 204 (2010) 3043–3046.
[12] C. Valero Vidal, A. Igual Muñoz, Electrochemical aspects in biomedical alloy characterization: electrochemical impedance spectroscopy, in: A. Laskovski (Ed.), Biomedical Engineering, Trends in Materials Science, InTech 2011, pp. 283–306.
[13] A. Igual Muñoz, L. Casabán Julián, Influence of electrochemical potential on the tribocorrosion behaviour of high carbon CoCrMo biomedical alloy in simulated body fluids by electrochemical impedance spectroscopy, Electrochim. Acta 55 (2010) 5428–5439.
[14] C. Valero Vidal, A. Igual Muñoz, Effect of thermal treatment and applied potential on the electrochemical behaviour of CoCrMo biomedical alloy, Electrochim. Acta 54 (2009) 1798–1809.
[15] L. Casabán Julián, A. Igual Muñoz, Influence of microstructure of HC CoCrMo biomedical alloys on the corrosion and wear behaviour in simulated body fluids, Tribol. Int. 44 (2011) 318–329.
[16] C. Valero Vidal, A. Igual Muñoz, Effect of physico-chemical properties of simulated body fluids on the electrochemical behaviour of CoCrMo alloy, Electrochim. Acta 56 (2011) 8239–8248.
[17] C. Valero Vidal, A. Igual Muñoz, Electrochemical characterisation of biomedical alloys for surgical implants in simulated body fluids, Corros. Sci. 50 (2008) 1954–1961.
[18] M.T. Mathew, M.J. Runa, M. Laurent, J.J. Jacobs, L.A. Rocha, M.A. Wimmer, Tribocorrosion behavior of CoCrMo alloy for hip prosthesis as a function of loads: a comparison between two testing systems, Wear 271 (2011) 1210–1219.
[19] J. Cassar, B. Mallia, A. Karl, J. Buhagiar, EIS of carburised CoCrMo: evolution of parameters characterising the metal-electrolyte interface, Surf. Coat. Technol. 292 (2016) 90–98.
[20] W. Stephen Tait, An Introduction to Electrochemical Testing for Practicing Engineers and Scientists, Pair O Docs Publications, USA, 1994.
[21] C. Fonseca, M.A. Barbosa, Corrosion behaviour of titanium in biofluids containing H_2O_2 studied by electrochemical impedance spectroscopy, Corros. Sci. 43 (2001) 547–559.
[22] M.E. Orazem, B. Tribollet, Electrochemical Impedance Spectroscopy, John Wiley & Sons Inc., NJ, USA, 2008.
[23] J.R. Davis, Corrosion: Understanding the Basics, ASM International, OH, USA, 2000.
[24] V.D. Jović, B.M. Jović, The influence of the conditions of the ZrO_2 passive film formation on its properties in 1 M NaOH, Corros. Sci. 50 (2008) 3063–3069.
[25] J. Geringer, J. Pellier, M.L. Taylor, D.D. Macdonald, Electrochemical impedance spectroscopy: insights for fretting corrosion experiments, Tribol. Int. 68 (2013) 67–76.
[26] M.T. Mathew, E. Ariza, L.A. Rocha, A.C. Fernandes, F. Vaz, TiC_xO_y thin films for decorative applications: tribocorrosion mechanisms and synergism, Tribol. Int. 41 (2008) 603–615.
[27] M.T. Mathew, E. Ariza, L.A. Rocha, F. Vaz, A.C. Fernandes, M.M. Stack, Tribocorrosion behaviour of TiC_xO_y thin films in bio-fluids, Electrochim. Acta 56 (2010) 929–937.